Primljen / Received: 1.11.2024.
Ispravljen / Corrected: 22.4.2025.
Prihvaćen / Accepted: 20.5.2025.
Dostupno online / Available online: 10.8.2025.

Bearing capacity of UHPC-filled circular steel tube short column under axial compression

Author:

Shengbing Fang, MCE
China Railway First Survey And Design Institute Group Co., Ltd. Xi'an China
15129367667@163.com
Corresponding author

Research Paper

Shengbing Fang

Bearing capacity of UHPC-filled circular steel tube short column under axial compression

This study establishes a predictive formula for the axial compression bearing capacity of Ultra High Performance Concrete (UHPC) filled circular steel tube (circular UHPCFST) short columns. The basis for establishing this formula is the derivation method of the axial compression-bearing capacity formula for common concrete-filled circular steel tube short columns and relevant research. To verify the rationality of the formula, a finite element model of the axial compression of circular UHPCFST short columns was established, and the current axial compression bearing capacity test values of the circular UHPCFST short columns were used for the simulation. These results indicate that the proposed formula can accurately predict the axial compression bearing capacity of circular UHPCFST short columns. Compared with the axial compression bearing capacity formula of circular UHPCFST short columns in other studies, the coefficient of variation of the formula in this study is reduced by 21.10 % to 115.73 %, which proves that the formula in this study is less discrete and has better applicability. It was found that the interaction between the steel tube and UHPC was desirable, and the increase in the diameter-thickness ratio weakened the composite action of the section.

Key words:

UHPC-filled steel tube, numerical simulation, finite element model, axial compression performance, ultimate bearing capacity

Prethodno priopćenje

Shengbing Fang

Nosivost kratkog stupa od kružnih čeličnih cijevi ispunjenih UHPC-om pod osnim tlakom

Ovo istraživanje predstavlja izraz za procjenu osne tlačne nosivosti kratkih stupova od kružnih čeličnih cijevi ispunjenih betonom vrlo visokih svojstava (kružni UHPCFST). Osnovu za utvrđivanje tog izraza čine postojeći izraz za određivanje osne tlačne nosivosti uobičajenih kratkih stupova od kružnih čeličnih cijevi ispunjenih betonom i relevantna prethodna istraživanja. Kako bi se provjerila prihvatljivost izraza, uspostavljen je model konačnih elemenata za simulaciju osnoga tlačnog ponašanja kratkih kružnih UHPCFST stupova, pri čemu su korišteni aktualni eksperimentalni podaci. Rezultati pokazuju da predloženi izraz može točno predvidjeti osnu tlačnu nosivost kratkih kružnih UHPCFST stupova. U usporedbi s izrazom za osnu tlačnu nosivost kratkih kružnih UHPCFST stupova u drugim istraživanjima, u ovom je istraživanju koeficijent varijacije smanjen za 21,10 do 115,73 %, što dokazuje da je izraz u ovome istraživanju manje diskretna i ima bolju primjenjivost. Utvrđeno je da je interakcija između čelične cijevi i UHPC-a poželjna, a povećanje omjera promjera i debljine dovodi do slabljenja međusobnog sprezanja.

Ključne riječi:
čelična cijev ispunjena UHPC-om, numerička simulacija, model konačnih elemenata, osni tlak, granična nosivost

1. Introduction

Concrete-filled steel tubes (CFST) are becoming increasingly popular in construction owing to their superior seismic performance, excellent bearing capacity, short construction period, and cost-effectiveness [1-9]. With the development of the social economy, the variety of super high-rise buildings, piers, and supporting systems that need to withstand ultra-high-pressure shrinkage loads or seismic loads is increasing. These have the characteristics of complex construction and high maintenance costs. The UHPCFST, which consists of a steel tube with ultra-high performance concrete, can address these problems because of its excellent comprehensive performance and remarkable durability [10, 11].

Recently, many researchers have studied ultra-high-performance concrete-filled steel tubes (UHPCFST) and made progress [12-16]. Researchers have found that the bearing capacity of UHPCFST short columns is mostly determined by the steel tube strength, section size, concrete strength, and steel tube thickness [17-19]. Guler et al. [20] conducted axial compression tests on circular UHPCFST short columns with the diameter-thickness ratio as the research parameter. The test results showed that when the thickness of the steel tube increases from 2.5 to 3.65 mm, the bearing capacity coefficient increases by an average of 5 %, and the ductility coefficient increases by an average of 69 %. Xu et al. [21] found that components with small confinement factors mainly underwent shear failures, while components with large confinement factors mainly underwent pier failures. The UHPCFST bearing capacity is closely correlated with the confinement factor and diameter-thickness ratio.

However, whether the current specification applies to UHPCFST remains to be studied [15, 19]. Huang et al. [22] compared the bearing capacity obtained by an ABAQUS simulation with the experimental value and found that the simulated value of the bearing capacity was more significant than the predicted value of the code formula. Hoang and Fehling [23] compared the test results with some current codes and found that EC4 overestimated the ultimate load of circular UHPCFST columns, while AISC and AIJ underestimated the ultimate load of circular UHPCFST columns.

To quantify the bearing capacity of UHPCFST, some scholars have analysed test data to obtain formulas [12, 14, 16]. Le Hoang and Fehling [24] performed a numerical simulation of short-circular UHPC-FSTCs, observed that thicker steel tubes and higher confinement factors exhibited better strength and ductility, and proposed a formula to predict the ultimate load and strain. Based on the results of regression analysis, Chen et al. [25] developed a formula for predicting the bearing capacity of UHPCFST. It was found that the yield strength of the steel and the diameter-thickness ratio of the steel tubes played decisive roles in the strength of the core UHPC.

This study pioneered a new approach for predicting the axial compressive bearing capacity of circular UHPCFST short columns. A novel predictor formula rooted in the limit equilibrium theory was developed and validated through ABAQUS finite element simulations, which elucidated the influence of the constraint coefficient and diameter-to-thickness ratio on the bearing capacity. The resulting formula exhibited enhanced applicability and accuracy compared with existing methods, marking a significant advancement in the field.

2. Formula derivation of axial compression bearing capacity

A schematic of the UHPC-filled circular steel tube short column used in this study is shown in Figure 1. a. According to the definition of short columns in the codes, columns with a length to diameter ratio of less than or equal to 4 (H/D≤4) are considered short columns.

In accordance with the formula for the axial compression bearing capacity of common CFST short columns, five unknown quantities affect the forces in the steel tubes and concrete cores: external load (N), longitudinal stress of the steel tube (σ_1), circumferential stress of the steel tube (σ_2), longitudinal stress of the concrete (σ_c), and lateral pressure (p) between the core concrete and steel tube [26]. As shown in Figure 1.b.

The compressive strength of concrete under triaxial compression is higher than that under uniaxial compression. According to the research conclusions, there is a linear relationship between the axial compression strength and lateral pressure under triaxial compression. Therefore, the relationship between the compression strength of UHPC under the steel tube constraint and that without lateral pressure can be written as

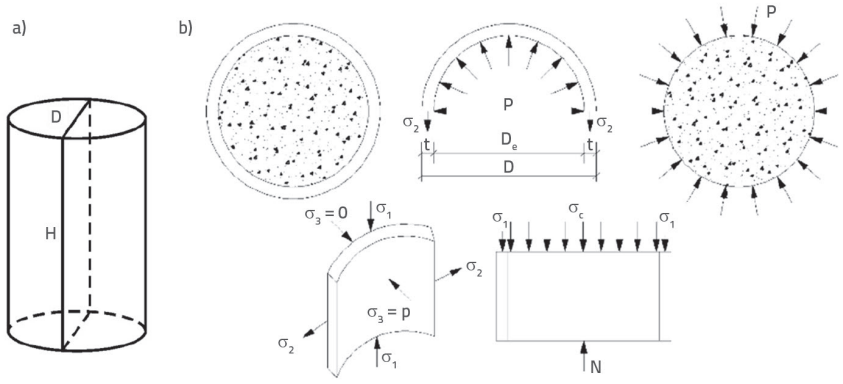

Figure 1. Short column of circular steel tube with UHPC: a) Schematic; b) Stress diagram

$$\sigma_c = f_c + K \cdot p \quad (1)$$

$$K = m + n / \sqrt{p / f_c} \quad (2)$$

where σ_c is the longitudinal stress of the concrete under the steel tube constraint, f_c is the axial compressive strength of the concrete without lateral pressure, K is the pressure measurement coefficient determined by the test, p is the lateral pressure between the core concrete and the steel tube, m and n are the coefficients of K.

Substituting Eq. (2) into Eq. (1), we obtain

$$\sigma_c = f_c\left(1+m\frac{p}{f_c}+n\sqrt{\frac{p}{f_c}}\right) \tag{3}$$

The steel tube adopts the Von Miss yield criterion, namely:

$$\sigma_1^2+\sigma_1\sigma_2+\sigma_2^2=f_y^2 \tag{4}$$

where f_y is the yield strength of steel.
From Figure 1, the static equilibrium equation is established:

$$N = A_c\sigma_c + A_s\sigma_1 \tag{5}$$

$$\sigma_2 t = \frac{D_c}{2}p \tag{6}$$

where A_s denotes the steel tube section area, A_c is the concrete section area, σ_1 is the longitudinal stress of the steel tube, t is the steel tube thickness, and D_c is the inner diameter of the steel tube.

Considering the small wall thickness of the steel tube, the following expression can be obtained:

$$\frac{A_s}{A_c}=\frac{4\pi D_c t}{\pi D_c^2}=\frac{4t}{D_c} \tag{7}$$

Linked by Eq.s. (3), (4), (6) and (7).

$$\sigma_1=\sqrt{f_y^2-3p^2\left(\frac{A_c}{A_s}\right)^2}-p\frac{A_c}{A_s} \tag{8}$$

Eq. (8) can be simplified as follows:

$$\sigma_1=\left(\sqrt{1-\frac{3}{\xi^2}\left(\frac{p}{f_c}\right)^2}-\frac{1}{\xi}\cdot\frac{p}{f_c}\right)f_y \tag{9}$$

where $\xi = (f_yA_s)/(f_cA_c)$ is called the confinement factor.

Substituting Eqs. (3) and (9) into (5), we obtaine *N*.

$$N=f_cA_c\left[1+\left(\sqrt{1-\frac{3}{\xi^2}\left(\frac{p}{f_c}\right)^2}+\frac{m}{\xi}\cdot\sqrt{\frac{p}{f_c}}+\frac{n-1}{\xi}\cdot\frac{p}{f_c}\right)\xi\right] \tag{10}$$

It can be seen from Eq. (9) that Eq. (10) is a functional expression of lateral pressure *p*. The derivative of the above formula and the corresponding lateral pressure *p** under the maximum load can be obtained from the extreme condition of $d_N/d_p = 0$.

$$\frac{1}{2}\cdot\frac{-\frac{6}{\xi^2}\cdot\frac{p^*}{f_c}}{\sqrt{1-\frac{3}{\xi^2}\left(\frac{p^*}{f_c}\right)^2}}+\frac{m}{2\xi\sqrt{\frac{p^*}{f_c}}}+\frac{n-1}{\xi}=0 \tag{11}$$

Eq. (11) can be simplified as follows:

$$\frac{3\frac{p^*}{f_c}}{\sqrt{\xi^2-3\left(\frac{p^*}{f_c}\right)^2}}-\frac{m}{2\sqrt{\frac{p^*}{f_c}}}-(n-1)=0 \tag{12}$$

Substituting p^*/f_c into Eq. (9), the predictor formula for the axial compression bearing capacity of circular UHPCFST short columns can be obtained as follows:

$$N=f_cA_c\left(1+a\sqrt{\xi}+b\xi\right) \tag{13}$$

where *a* and *b* are the coefficient of *m* and *n*.

3. Numerical simulations of bearing capacity

To obtain the formula coefficients a and b, a numerical analysis was conducted using the ABAQUS software, and the numerical simulation results were fitted.

3.1. Simulation method

To make the finite element model closer to the actual component, the upper and lower end plates were set to simulate the loading plate of the test press, so that the error was smaller. A short column with end plates is shown in Figure 2.

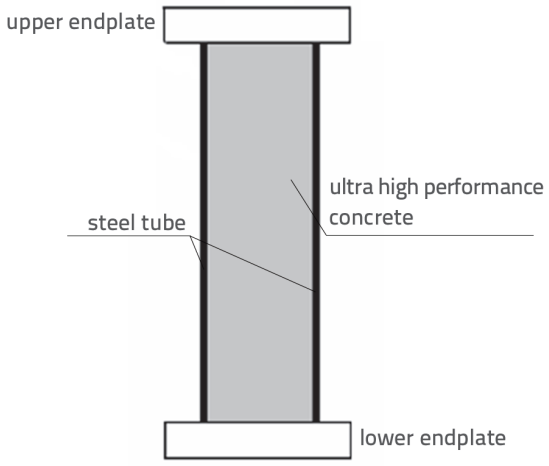

Figure 2. Short column with upper and lower endplates

In addition, the upper and lower endplates were regarded as rigid bodies without considering the influence of endplate deformation on the simulation results. The steel tube, UHPC, and endplate components adopt a three-dimensional solid eight-node reduced integral element (C3D8R). During the loading process, there was no slip between the endplate and steel tube or between the endplate and UHPC. Therefore, the top and bottom surfaces of the circular steel tubular stub columns were fixed in all degrees of freedom except for the top

surface displacement in the Z-axis direction. The interaction between the steel tube and UHPC primarily includes normal and tangential effects, and normal contact is difficult. The tangential contact is the mechanical friction expressed by the Coulomb friction model, and the friction coefficient is 0.3.

3.2. Material model

3.2.1. Material model of steel

In this study, the ideal elastic-plastic model is adopted, which not only meets the calculation accuracy but also saves computer resources and reduces the calculation time of the model. The expressions for the ideal elastic-plastic model are shown in Eq. (14).

$$\begin{aligned} \sigma_s &= E_s\varepsilon_s \qquad \varepsilon_s \le \varepsilon_y \\ \sigma_s &= f_y \qquad \varepsilon_s \ge \varepsilon_y \end{aligned} \tag{14}$$

where E_s is the elastic modulus of the steel, σ_s is the steel stress, ε_s is the steel strain, ε_y is the steel yield strain, and f_y is the steel yield stress.

3.2.2. Material model of concrete

The core concrete model of Han Linhai's constitutive model was used in this study. Furthermore, the simulation results of this model reflect the actual mechanical behaviour of the members. Linhai's constitutive model is shown in Equations (15) and (16).

$$y = 2x - x^2 \qquad (x \le 1) \tag{15}$$

$$y = \begin{cases} 1 + q\cdot(x^{0.1\xi} - 1) & (\xi \ge 1.12) \\ \dfrac{x}{\beta\cdot(x-1)^2 + x} & (\xi < 1.12) \end{cases} \qquad (x > 1)$$

$$\sigma_0 = \left[1 + \left(-0.054\cdot\xi^2 + 0.4\cdot\xi\right)\cdot\left(\frac{24}{f_c}\right)^{0.45}\right]\cdot f_c$$

$$\varepsilon_0 = \varepsilon_{cc} + \left[1400 + 800\cdot\left(\frac{f_c}{24} - 1\right)\right]\cdot\xi^{0.2}\,(\mu\varepsilon) \tag{16}$$

$$\varepsilon_{cc} = 1300 + 12.5\cdot f_c\,(\mu\varepsilon)$$

$$\beta = \left(2.36\times10^{-5}\right)^{\left[0.25+(\xi-0.5)^7\right]}\cdot f_c^{\,2}\cdot 3.51\times10^{-4}$$

$$q = \frac{\xi^{0.45}}{2+\xi}; \qquad x = \frac{\varepsilon}{\varepsilon_0}; \qquad y = \frac{\sigma}{\sigma_0}$$

where σ_0 is the peak stress of concrete, ε_0 is the peak strain of concrete, σ is the stress of concrete, ε is the strain of concrete, ξ is the constraint coefficient of concrete-filled steel tube, x is the ratio of ε to ε_0, y is the ratio of σ to σ_0, q is a coefficient with regard to ξ, and β is a coefficient with regard to ξ and f_c.

3.3. Numerical simulation

3.3.1. Numerical simulation process

The elastic modulus and Poisson's ratio of the steel pipe were set to 206000 MPa and 0.3, respectively. The elastic modulus of the UHPC was calculated according to the following equation, and the Poisson's ratio was taken as 0.2.

$$E_c = 0{,}2501\sqrt{f_c} + 1{,}446)\times 10^4$$

To ensure that the characteristics of the upper and lower endplates in the model were consistent with those of the upper and lower metal pads of the press; the upper and lower endplates were treated as rigid bodies. That is, the influence of end-plate deformation on the simulation results was not considered. Therefore, the end plate is only given an elastic modulus and is set sufficiently large, whereas Poisson's ratio is set sufficiently small. In this study, the elastic moduli of the upper and lower end plates to 206000000 MPa and Poisson's ratio to 0.0001.

The appropriate setting of the analysis steps has a significant impact on the convergence of the model. The step size is small, and the number of steps that must be calculated increases. The number of computations also increased. Therefore, smaller step sizes do not necessarily guarantee better results. A step size that is too small requires too many computer resources and may not have much meaning. The settings of the step parameters analysed in this study are listed in Table 1.

When dividing the grid, complex models can be segmented first and the number of seeds can be increased in the key analysis and stress concentration areas to satisfy the requirements of the key analysis area for the number of grids. In other nonkey analysis areas, the number of seeds can be appropriately reduced to reduce the number of grids. Therefore, the first step was to cut the steel pipe and UHPC components to make the mesh division between them steel pipe and UHPC more uniform. The three-dimensional mesh division of each component in the round steel-pipe UHPC short column is shown in Figure 3.

Table 1. Analysis step parameter settings

Time duration	Maximum incremental steps	Incremental step size		
		Initial incremental step	Minimum incremental step	Maximum incremental step
1	1000	0.01	$1\cdot10^{-5}$	0.1

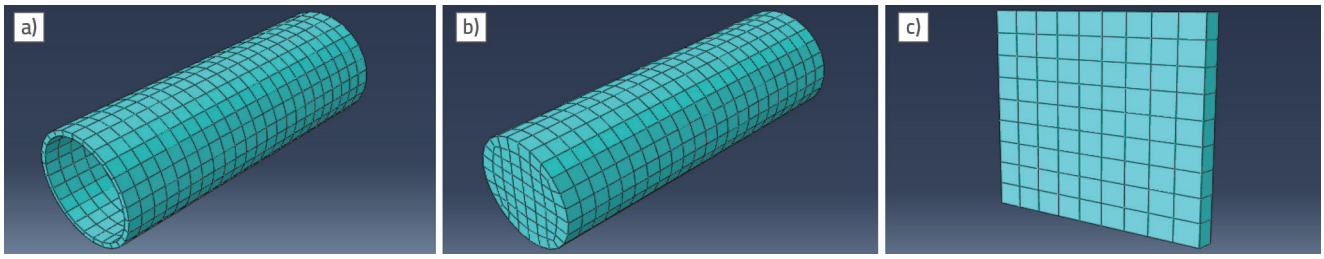

Figure 3. Three-dimensional mesh division diagram of steel pipe UHPC short column components: a) Grid division diagram of steel pipe; b) UHPC Grid partition diagram; c) End-plate grid division diagram

During the loading process, owing to the absence of slip between the end plate and steel pipe, as well as between the end plate and UHPC, tight contact was maintained. Therefore, the contact between the end plate and steel pipe, as well as between the end plate and UHPC, is in the form of binding. Simultaneously, the end plate was set as the main surface, and the steel pipe and concrete end faces were set as secondary surfaces.

The normal direction of the interface between the steel pipe and UHPC was in contact. This approach can be described using ABAQUS, which applies contact constraints between the steel pipe and the UHPC only when the gap between the two contact surfaces is zero. There is no limitation on the magnitude of the contact pressure that can be transmitted between the two contact surfaces; that is, the pressure perpendicular to the contact surface can be completely transmitted between the interfaces. When the pressure between the contact surfaces is zero or negative, separation occurs between the two contact surfaces, indicating constraint failure.

The Coulomb friction model was used for the tangential direction of the interface between the steel pipes and UHPC. The normal pressure on the two contact surfaces directly affects the critical shear stress. The relationship between the two can be expressed by the following equation:

$$\tau_{crit} = \mu p$$

The friction behaviour between two contact surfaces is represented by the friction coefficient μ, where p is the normal contact pressure between the two contact surfaces. The friction coefficient between steel pipes and concrete typically ranges from 0.2 to 0.6. After the calculation, the friction coefficient in this study was set to 0.3.

All the models in this study were equipped with endplates. The main reason for this was to make the finite element model closer to the actual components by setting up the upper and lower end plates to simulate the loading plate of the test press to minimise errors. Second, stress concentration on the surface of the component is prevented owing to the software's own reasons, which may cause the loading method of the simulated steel pipe UHPC short column to be inconsistent with the ideal loading method.

3.3.2. Numerical simulation results

ABAQUS established an axial compression model of 63 circular UHPCFST short columns, and the simulated bearing capacity values are listed in Table 2.

In Table 2, the first parameter is the thickness of the steel tube, denoted by T3, T5, T6, and T7, representing thicknesses of 3, 5, 6, and 7 mm, respectively. The second parameter is the yield strength of the steel, denoted as S1, S2, S3, and S4, which represent yield strengths of 235, 300, 345, and 390 MPa, respectively. The third parameter is the axial compression strength of the concrete, denoted by C1, C2, C3, and C4, which represent concrete strengths of 100, 120, 130, and 150 MPa, respectively. The fourth parameter is the diameter of the circular steel tube, denoted by 9, 11, 13, and 16, representing diameters of 90, 113, 135, and 169 mm, respectively. For example, T3-S1-C1-11 is a circular section member with a steel thickness of 3 mm, concrete axial compression strength of 100 MPa, steel yield strength of 235 MPa, and a diameter of 113 mm. Here, D represents the diameter of the circular section. The length-to-diameter ratios of the members are 3. *NE* is the simulated value of the axial compression bearing capacity of the UHPCFST short columns, *N*0 is the nominal bearing capacity, *N*0 = *fyAs* + *fcAc*. CCR is the concrete contribution rate, which is the ratio of *NE* to the steel tube bearing capacity. It is calculated by Eq. (17).

$$\mathrm{CCR} = \frac{N_E}{N_H} \tag{17}$$

where N_H is steel tube bearing capacity value, and $N_H = f_y A_s$.

SI is the strength index of the UHPCFST, which is the ratio of N_E to N_0, and is calculated using Eq. (18).

$$\mathrm{SI} = \frac{N_E}{N_0} \tag{18}$$

3.4 Formula coefficient fitting

Based on the data in Table 2, the approximate values of *a* and *b* in Eq. (13) are obtained using the linear regression method in the Origin software. As shown in Figure 4, a = 0.04765, b = 1.49501. Therefore, the coefficient of the prediction formula after fitting Eq. (13) is:

$$N = f_c A_c \left(1 + 0.04765\sqrt{\xi} + 1.49501\xi\right) \tag{19}$$

Table 2. Details of UHPCFST specimens

Specimen	D/t	ξ	N_E [kN]	N_0 [kN]	CCR	SI	Specimen	D/T	ξ	N_E [kN]	N_0 [kN]	CCR	SI
T3-S1-C1-11	37.7	0.27	1312	1143	5.385	1.148	T6-S1-C3-11	18.8	0.46	1776	1516	3.747	1.172
T3-S1-C2-11	37.7	0.23	1474	1323	6.050	1.114	T6-S1-C4-11	18.8	0.39	1924	1676	4.059	1.148
T3-S2-C1-11	37.7	0.35	1410	1210	4.534	1.165	T6-S2-C3-11	18.8	0.58	1957	1647	3.234	1.189
T3-S2-C2-11	37.7	0.29	1587	1390	5.103	1.142	T6-S2-C4-11	18.8	0.50	2138	1807	3.533	1.183
T3-S2-C3-11	37.7	0.27	1671	1480	5.373	1.129	T6-S3-C1-11	18.8	0.87	1892	1497	2.719	1.264
T3-S2-C4-11	37.7	0.23	1833	1660	5.894	1.104	T6-S3-C2-11	18.8	0.72	2033	1657	2.922	1.227
T3-S3-C1-11	37.7	0.40	1490	1257	4.166	1.185	T6-S3-C3-11	18.8	0.67	2107	1737	3.028	1.213
T3-S3-C2-11	37.7	0.33	1651	1437	4.616	1.149	T6-S3-C4-11	18.8	0.58	2248	1898	3.231	1.185
T3-S3-C3-11	37.7	0.31	1748	1527	4.887	1.145	T6-S4-C1-11	18.8	0.98	2047	1588	2.602	1.289
T3-S3-C4-11	37.7	0.27	1917	1707	5.360	1.123	T6-S4-C2-11	18.8	0.82	2170	1748	2.759	1.241
T3-S4-C1-11	37.7	0.45	1564	1304	3.868	1.200	T6-S4-C3-11	18.8	0.76	2241	1828	2.849	1.226
T3-S4-C2-11	37.7	0.38	1723	1483	4.261	1.162	T6-S4-C4-11	18.8	0.66	2389	1988	3.037	1.201
T3-S4-C3-11	37.7	0.35	1820	1573	4.501	1.157	T7-S1-C1-11	16.1	0.71	1631	1318	2.977	1.238
T3-S4-C4-11	37.7	0.30	1989	1753	4.919	1.135	T7-S1-C2-11	16.1	0.59	1776	1472	3.242	1.207
T5-S1-C1-11	22.6	0.48	1474	1232	3.697	1.197	T7-S1-C3-11	16.1	0.55	1847	1549	3.372	1.193
T5-S1-C2-11	22.6	0.40	1639	1399	4.111	1.172	T7-S1-C4-11	16.1	0.47	1978	1703	3.611	1.162
T5-S1-C3-11	22.6	0.37	1703	1482	4.272	1.149	T7-S2-C1-11	16.1	0.91	1870	1469	2.674	1.273
T5-S1-C4-11	22.6	0.32	1862	1649	4.671	1.130	T7-S2-C2-11	16.1	0.76	1995	1623	2.853	1.229
T5-S2-C1-11	22.6	0.61	1654	1342	3.250	1.232	T7-S2-C3-11	16.1	0.70	2053	1700	2.936	1.208
T5-S2-C2-11	22.6	0.51	1797	1509	3.531	1.191	T7-S2-C4-11	16.1	0.61	2198	1854	3.143	1.186
T5-S2-C3-11	22.6	0.47	1885	1592	3.704	1.184	T7-S3-C1-11	16.1	1.05	2042	1574	2.539	1.297
T5-S2-C4-11	22.6	0.41	2043	1759	4.014	1.162	T7-S3-C2-11	16.1	0.87	2139	1728	2.660	1.238
T5-S3-C1-11	22.6	0.70	1754	1419	2.997	1.237	T7-S3-C3-11	16.1	0.80	2209	1805	2.747	1.224
T5-S3-C2-11	22.6	0.59	1917	1585	3.275	1.209	T7-S3-C4-11	16.1	0.70	2352	1959	2.925	1.201
T5-S3-C3-11	22.6	0.54	1993	1669	3.405	1.195	T7-S4-C1-11	16.1	1.18	2200	1679	2.420	1.310
T5-S3-C4-11	22.6	0.47	2148	1835	3.670	1.170	T7-S4-C2-11	16.1	0.98	2308	1833	2.539	1.259
T5-S4-C1-11	22.6	0.79	1884	1495	2.848	1.260	T7-S4-C3-11	16.1	0.91	2364	1910	2.600	1.238
T5-S4-C2-11	22.6	0.66	2020	1662	3.053	1.216	T7-S4-C4-11	16.1	0.79	2507	2064	2.758	1.215
T5-S4-C3-11	22.6	0.61	2099	1745	3.173	1.203	T5-S3-C1-9	18.0	0.92	1219	963	2.646	1.265
T5-S4-C4-11	22.6	0.53	2259	1912	3.414	1.182	T5-S3-C1-13	27.0	0.57	2368	1932	3.361	1.226
T6-S1-C1-11	18.8	0.59	1569	1275	3.310	1.230	T5-S3-C1-16	33.8	0.45	3427	2874	3.856	1.192
T6-S1-C2-11	18.8	0.49	1706	1435	3.599	1.189							

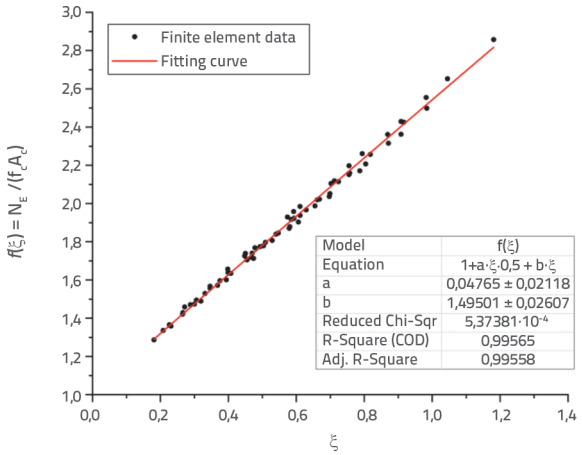

Figure 4. Coefficient fitting

3.5. Formula validation

The test results of the 78 experimental samples in Table 3 were collected to evaluate the calculation formula [21, 27, 28]. The collected test data satisfied the following requirements:

- the core concrete was UHPC,
- the length-to-diameter ratio was less than four,
- the specimen was tested under an axial static load.

There is no limitation on the strength of the steel when developing a predictor formula with a wider scope of application. Based on the data in Table 3, the bearing capacity of each tested member was calculated using Eq. (19). The differences between the predicted and experimental values of the bearing capacity formula were plotted. This

Table 3. Collected data of HUPCFST

Source	D [mm]	t [mm]	D/t	L [mm]	L/D	f_y [MPa]	f_c [MPa]	ξ	Number
Xu (2019) [21]	108	3.5-12	9-30.9	324	3	351-430	90-130	0.55-3.11	37
Lin (2004) [27]	133	3-12	11.1-44.3	400	3	290-376	109-154	0.18-1.33	22
Feng (2008) [28]	108-113	5-6.5	17.4-22	300	2.7-2.8	310-391	116-145	0.46-0.77	19

is illustrated in Fig. 5. Generally, the data obtained from the bearing-capacity formula agreed with the experimental data. Additionally, the errors were mostly within 10 %, which is acceptable. Therefore, it is feasible to calculate the axial compression bearing capacity of the UHPCFST short columns using Eq. (19) and the calculation results of Eqs. (19) can better reflect the axial compression bearing capacity of the actual members.

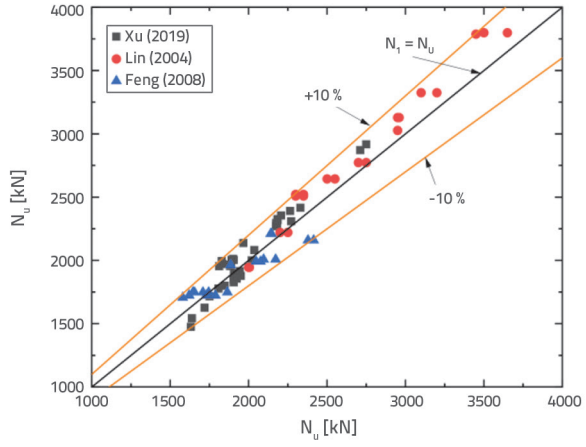

Figure 5. Comparison between the predicted values of the formula and the collected test values

4. Discussion on the compression properties of UHPCFST short columns

The finite element models of the UHPCFST short columns before and after loading are shown in Figure 6. As shown in Figure 6.b, a slight swelling is observed in the middle of the tube after loading. Subsequently, the compressive properties are discussed.

4.1. Stress distribution

Figure 7 illustrates the distribution of the longitudinal stress (S33) of UHPC during the loading process of the examples (from a to d). At the beginning of the loading, the longitudinal stress of the UHPC section was uniformly distributed (Figure 7.a), indicating that the UHPC was still in an elastic state. Figure 7.b shows the stress distribution when the specimen reaches its ultimate bearing capacity. As shown, the stress value in the core area was higher than that at the periphery. The stress decreases from the core area to the periphery, and the stress on the concrete is uniform in the circumferential direction. As shown in Figure 7.c, after the specimen passed through the ultimate stress, the longitudinal stress of the concrete at the centre of the section was still high owing to the uniform steel tube constraint. In Figure 7.d, the concrete near the edge was generally crushed at the end of the loading, and the residual stress was small; however, the central region still presented a high longitudinal stress.

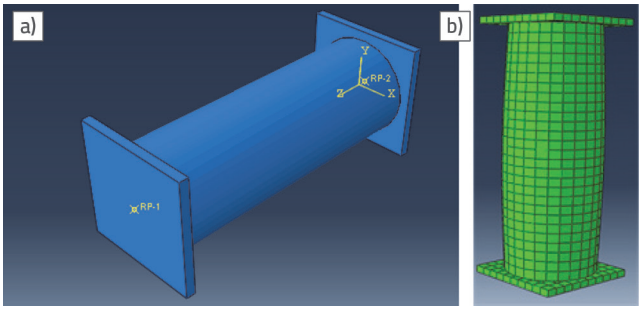

Figure 6. The finite element model diagrams: a) Before loading; b) After loading

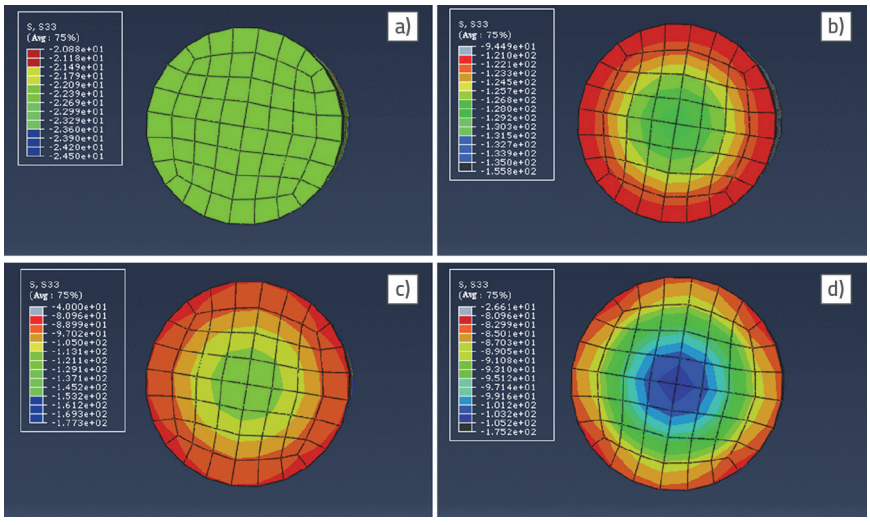

Figure 7. Distribution of vertical stress of UHPC at the mid-span section

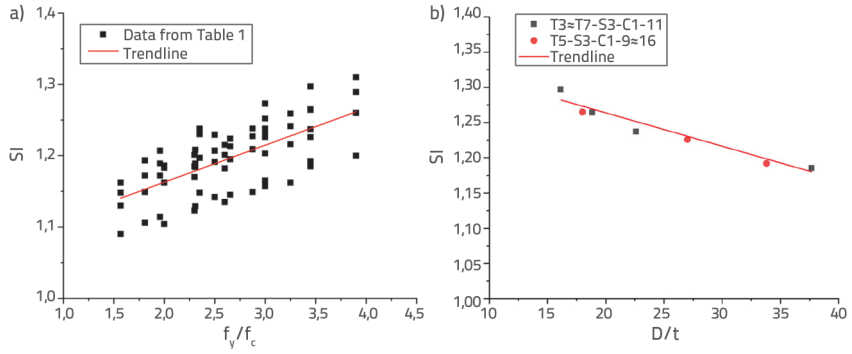

Figure 8. Effect of the f_y/f_c and D/t on SI

4.3. Concrete contribution rate

The contribution concrete rate (CCR) is defined as the strengthening effect of the core concrete on the UHPCFST. Figure 9 shows the CCR and diameter-thickness ratio, concrete strength, and confinement factor diagrams. Figure 9 shows that the CCR increases with the diameter–thickness ratio, increases with the advancement of concrete strength, and decreases with the advancement of the confinement factor. This was because, as the diameter-thickness ratio of the steel tubes increased, the steel tube was more likely to buckle locally, weakening its constraint effects on the core concrete. To quantify the relationship between the CCR and the confinement factor, a regression analysis of the data in Figure 9.c is carried out, and Eq. (20) is obtained.

4.4. Bearing capacity impact analysis

Figure 10 shows the relationship between the axial compression bearing capacity of UHPCFST short columns and the influencing parameters. As shown in Figure 10, under the influence of the same parameters, each curve exhibits a similar trend.

Figure 10.a is the relationship between bearing capacity and concrete strength. Bearing capacity increased by 22.46 percent from 1754 kN to 2148 kN, when the strength of concrete increased by 50.0 % from 100 MPa to 150 MPa. That is, the growth of bearing capacity corresponding to every 1 % increase in concrete strength is 0.45 %.

Figure 10.b is the relationship between bearing capacity and steel tube strength. Steel tube strength increased from 235 MPa to 390 MPa, with an increase of 65.96 %; the bearing capacity increased from 1474 kN to 1884 kN, with an increase of 27.82 %. That is, the corresponding bearing capacity increases by 0.42 % for every 1 % increase in the strength of the steel tube.

Figure 10.c shows the relationship between the bearing capacity and steel tube thickness. For the thicknesses of 3, 5, 6, and 7 mm, the corresponding bearing capacities were 1490, 1754, 1892, and 2042 kN, respectively. Based on the steel tube thickness of 3 mm members, the thickness of 5 mm, 6 mm, and 7mm members increased by 66.67 %, 100.00 %, and 133.33 %, respectively, and the bearing capacity increased by17.72 %, 26.98 %, and 37.05 %, respectively. When the steel tube thickness increased by 1 %, the bearing capacity increased by 0.27 %, 0.27 %, and 0.28 %, respectively.

Figure 10(d) shows the relationship between the bearing capacity and section size. The ultimate bearing capacity increased significantly with an increase in section size. The bearing capacities of the members with diameters of 90, 113, 135, and 169 mm are 1219 kN, 1754, 2368, and 3427 kN, respectively. The component with a diameter of 90 mm was taken as the benchmark. The diameters of the components with diameters of 113 mm, 135 mm, and 169 mm increased by 25.56 %, 50 %, and 87.78 %, respectively, and the bearing capacities increased by 43.89 %, 94.26 %, and 181.13 %, respectively. For every 1 % increase in the diameter of the component, the bearing capacity increased by 1.72 %, 1.89 %, and 2.06 %, respectively.

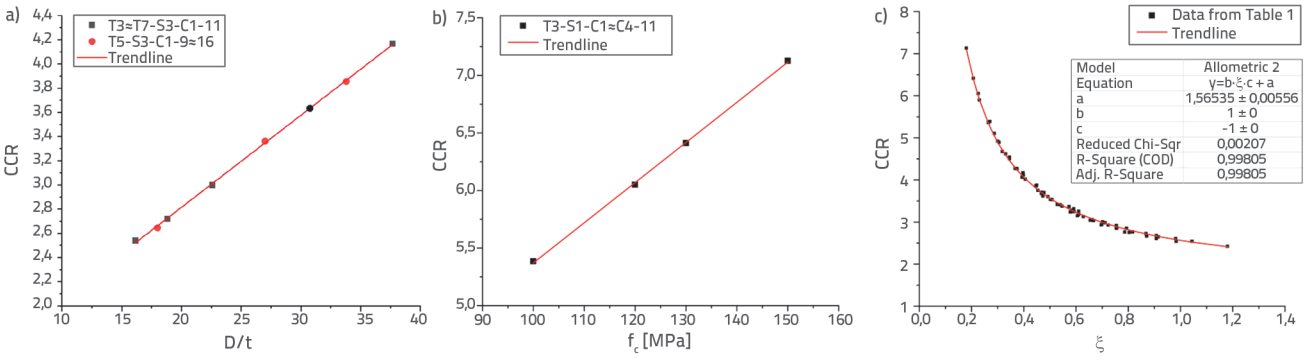

Figure 9. Effect of D/t, concrete strength f_c and confinement factor ξ on contribution concrete rate (CCR): a) D/t; b) Concrete strength f_c; c) Confinement factor ξ

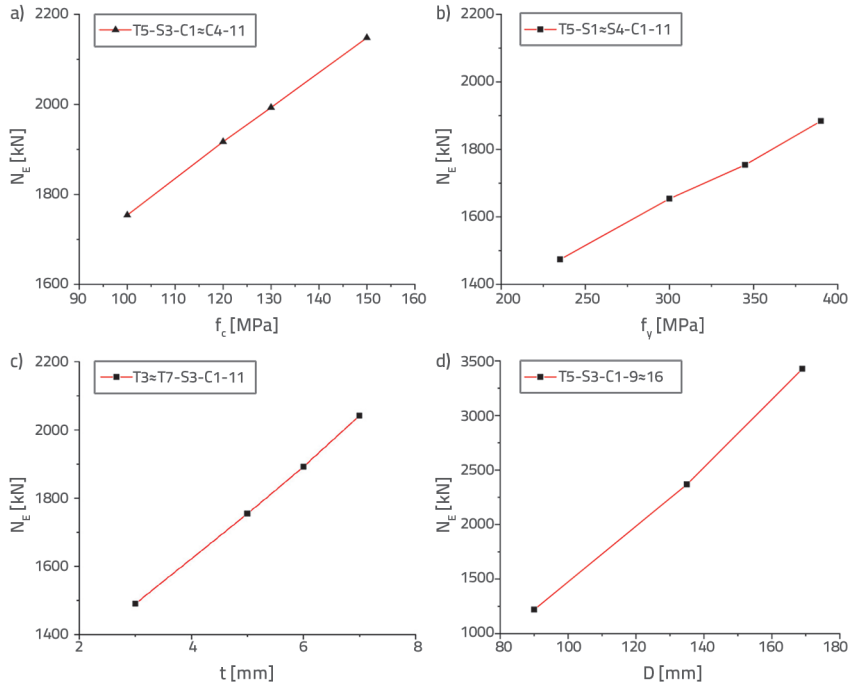

Figure 10. Effects of concrete strength, steel tube strength, steel tube thickness, and section size on bearing capacity (N_E): a) Concrete strength f_c; b) Steel tube strength f_y; c) Steel tube thickness t; d) Section size D

In addition, Table 3 shows that the strength ranges for the steel tubes were 290 to 430 MPa, for concrete 90 to 154 MPa, and for the confinement factor 0.18 to 3.11.

Therefore, the bearing capacity formula in this study can be applied not only to the bearing capacity calculation of steel tube strength in the range of 235 to 390 MPa and confinement factor in the range of 0.18 to 1.18 but also to steel tubes and concrete with higher strength.

5. Comparison and discussions

Based on the collected experimental data, the bearing capacity of each tested member was calculated using the bearing capacity formula proposed in this study and other formulae (Table 4). The mean value and variation coefficient of the ratio of the predicted value of each formula to the experimental value are summarised in Table 5. It can be seen from Table 5, the prediction error provided by Rong et al. [29] was within 10 %, and the prediction errors of other formulas were within 5 %. This indicates that Rong et al. [29] underestimated the ultimate load capacity of UHPCFST. Therefore, some of the material properties are wasted and are not economical. The predicted results of Eqs. (19) were 2.7 % higher than the test results, indicating a slight overestimation. The error between the predicted results and the test results provided by Chen et al. [25] was only 0.9 %, and the predicted results were the best. However, the coefficient of variation indicated that the prediction results obtained by Chen et al. [25] were the most unstable, and the coefficient of variation of the ratio of the predicted value to the experimental value in this study was the smallest. Compared with the coefficient of variation of the formula in this study, the coefficient of variation error of Rong et al. [29] larger 21.10 %, Chen et al. [17] larger 115.73 %, Wu and Lin [30] larger 67.37 %, indicating that the predictive value of Eq. (19) is less discrete and less accurate. Therefore, Eq. (19) is applicable for predicting the axial compression bearing capacity of the UHPCFST short columns.

Table 4. Selected predictor formulas of axial compression bearing capacity of circular UHPCFST short columns

Authors	Expressions	Notations
Rong (2018) [29]	$N = f_c A_c(1+1{,}25\xi)$	f_c - the axial compression strength of concrete
Chen (2018) [25]	$N_u = f_c A_c + (1+k) f_c A_c$ $k = 0{,}17 - 0{,}0013D/t\sqrt{f_y}/235$	k - the strengthening coefficient, which reflects the strengthening effect of steel tubes on the strength of core UHPC
Wu & Lin (2005) [30]	$N = f_y A_s + f_{co} A_c$ $f_{co} = f_c[1{,}2 + 0{,}25(100/f_c)1{,}25\xi 2\text{-}0{,}04\xi]$	f_{co} - the uniaxial compression strength of core concrete considering the constraint effect

Table 5. Comparison between the predicted values of this formula and other formulas

	Result	Rong (2018) [29]	Chen (2018) [25]	Wu & Lin (2005) [30]	Eq. (19)
N_t/N_p	Mean value	0.921	0.991	1.016	1.027
	Coefficient of variation	0.064	0.113	0.088	0.053
	(A-B)/B	21.10 %	115.73%	67.37 %	0.00 %
Note: N_t is the bearing capacity of the test components listed in Table 2, and N_{tp} is the predicted value of the bearing capacity of the test member. where A is the coefficient of variation of Rong, Chen, Wu, and Lin, and B is the coefficient of variation of Eq. (17).					

6. Conclusion

This study theoretically derived a predictor formula for the axial compression-bearing capacity of UHPCFST short columns. The formula coefficients *a* and *b* were obtained through numerical simulation tests using the finite element software ABAQUS. The predicted values of the formula were compared with those of other formulas, and the following conclusions were drawn:

- Circular UHPCFST short columns were analysed and studied based on the limit equilibrium theory. A prediction formula for the axial compression bearing capacity of circular UHPCFST short columns was proposed, including the diameter-thickness ratio of the steel tube and the coefficient factor.
- The feasibility of the formula was validated based on the collected experimental data, and the formula was compared with other formulas. The results showed that the predictive value of this formula is less discrete, has higher accuracy, and is more applicable.
- Increases in the diameter-thickness ratio weakened the composite action of the section, whereas increases in f_y/f_c strengthened it.
- The CCR increases with the diameter–thickness ratio, increases with the concrete strength, and decreases with the confinement factor. A formula was established to predict the CCR based on the coefficient factor.
- The formula in the current code for concrete-filled steel is only suitable for calculating concrete-filled steel tubes with concrete strength levels lower than C100. The formula obtained in this study is specific to concrete-filled steel tubes with ultra-high-strength concrete (strength levels higher than C100), which fills the gap in the current research.

The formula obtained in this study has a smaller dispersion, higher accuracy, and wider application range, which can better predict the axial compression bearing capacity of UHPCFST and provide a theoretical calculation basis for the design of UHPCFST. However, in real-world engineering applications, UHPCFST members are also subjected to loading conditions such as axial compression combined with moment and shear force, and tension force combined with moment and shear force. Future research will focus on these loading scenarios to further improve the accuracy and practicality of the proposed formulae. In addition, the formula used in this study is only applicable to short columns. In subsequent research, it will be necessary to consider the influence of stability and to study the calculation formula for the bearing capacity of slender columns.

Acknowledgements

This research was supported by the Chongqing Technology Innovation and Application Development Special General Project (cstc2020jscx-msxmX0084), Chongqing Construction Science and Technology Plan Key Project (Urban Science 2021, No. 1-8), and Research Project of Guangzhou Education Bureau (2024312467).

REFERENCES

[1] Patel, V., Liang, Q., Hadi, M.: Nonlinear analysis of axially loaded circular concrete-filled stainless steel tubular short columns, J CONSTR STEEL RES, 11 (2014), pp. 9-18, https://doi.org/10.1016/j.jcsr.2014.04.036

[2] Han, L., Li, W., Bjorhovde, R.: Developments and advanced applications of concrete-filled steel tubular (CFST) structures: Members, J CONSTR STEEL RES, 100 (2014), pp. 211-228, https://doi.org/10.1016/j.jcsr.2014.04.016

[3] Patel, V., Uy, B., Prajwal, K., et al.: Confined concrete model of circular, elliptical and octagonal CFST short columns, STEEL COMPOS STRUCT, 22 (2016) 3, pp. 497-520, https://doi.org/10.12989/scs.2016.22.3.497

[4] Liew, J., Xiong, M., Xiong, D.: Design of Concrete Filled Tubular Beam-columns with High Strength Steel and Concrete, STRUCTURES, 8 (2016), pp. 213-226, https://doi.org/10.1016/j.istruc.2016.05.005

[5] Zheng, J., Wang, J.: Concrete-Filled Steel Tube Arch Bridges in China, ENGINEERING-PRC, 4 (2018) 1, pp. 143-155, https://doi.org/10.1016/j.eng.2017.12.003

[6] Gunawardena, Y., Aslani, F., Uy, B.: Review of strength behaviour of circular concrete filled steel tubes under monotonic pure bending, J CONSTR STEEL RES, 158 (2019), pp. 460-474, https://doi.org/10.1016/j.jcsr.2019.04.010

[7] Xie, K., Wang, H., Pang, J., et al.: Study of the Ultimate Bearing Capacity of Concrete-filled Steel Tube K-Joints, KSCE J CIV ENG, 23 (2019) 5, pp. 2254-2262, https://doi.org/10.1007/s12205-019-1268-7

[8] Zhu, H., Zhang, H., Liu, L.: Experimental Study on Cyclic Lateral Loaded Circular CFST Members with Initial Imperfections, KSCE J CIV ENG, 25 (2021) 8, pp. 3064-6074, https://doi.org/10.1007/s12205-021-1931-7

[9] Almasslawi, A., Ekmekyapar, T., Al-Eliwi, B.: Repair of Buckled Concrete Filled Steel Tube Columns Subjected to Axial Compression, KSCE J CIV ENG, 24 (2020) 5, pp. 1499-1508, https://doi.org/10.1007/s12205-020-0321-x

[10] Hoang, A., Fehling, E.: A review and analysis of circular UHPC filled steel tube columns under axial loading, STRUCT ENG MECH, 62 (2017) 4, pp. 417-430, https://doi.org/10.12989/sem.2017.62.4.417

[11] Liew, J., Xiong, D.: Ultra-High Strength Concrete Filled Composite Columns for Multi-Storey Building Construction, ADV STRUCT ENG, 15 (2012) 9, pp. 1487-1503, https://doi.org/10.1260/1369-4332.15.9.1487

[12] Yu, C., Yu, M., Xu, L., et al.: Experimental investigation of the behavior of UHPCFST under repeated axial tension, ENG STRUCT, 314 (2024) 118293, https://doi.org/10.1016/j.engstruct.2024.118293

[13] Yu, M., Liao, W., Liu, S., et al.: Axial compressive performance of ultra-high performance concrete-filled steel tube stub columns at different concrete age, STRUCTURES, 55 (2023), pp. 664-676, https://doi.org/10.1016/j.istruc.2023.05.113

[14] Zhao, Z., Wei, Y., Wang, G., et al.: Axial compression performance of square UHPC-filled stainless-steel tubular columns, CONSTR BUILD MATER, 408 (2023) 133622, https://doi.org/10.1016/j.conbuildmat.2023.133622

[15] Cai, H., Zeng, Y., Xu, L., et al.: Axial behavior of ultra-high performance steel fiber reinforced concrete filled circular steel tubular columns, STRUCTURES, 68 (2024) 107186, https://doi.org/10.1016/j.istruc.2024.107186

[16] Li, J., Deng, Z.: Performance of square UHPC filled high-strength steel tubular columns under axial compression: Experiment and theory analysis, STRUCTURES, 46 (2022), pp. 1395-1406, https://doi.org/10.1016/j.istruc.2022.11.019

[17] Yu, C., Yu, M., Xu, L., et al.: Experimental research on mechanical behavior of UHPCFST under repeated axial compression, J CONSTR STEEL RES, 218 (2024) 108690,https://doi.org/10.1016/j.jcsr.2024.108690

[18] Wu, F., Xu, L., Zeng, Y., et al.: Experimental investigation of axially loaded circular ultra-high performance concrete with coarse aggregate (CA-UHPC) filled steel tube slender columns, STRUCTURES, 58 (2024) 105355, https://doi.org/10.1016/j.istruc.2023.105355

[19] Ren, Z., Wang, D., Kondo, G.: Axial compressive capacity prediction and optimal design of circular UHPC-filled steel tube based on Hybrid Symbolic Regression - Neural Network model, STRUCTURES, 68 (2024) 107084, https://doi.org/10.1016/j.istruc.2024.107084

[20] Guler, S., Çopur, A., Aydogan, M.: Axial capacity and ductility of circular UHPC-filled steel tube columns, MAG CONCRETE RES, 65 (2013) 15, pp. 898-905, https://doi.org/10.1680/macr.12.00211

[21] Xu, L., Lu, Q., Chi, Y., et al.: Axial compressive performance of UHPC filled steel tube stub columns containing steel-polypropylene hybrid fiber, Constr Build Mater, 204 (2019), pp. 754-767, https://doi.org/10.1016/j.conbuildmat.2019.01.202

[22] Huang, W., Fan, Z., Shen, P., et al.: Experimental and numerical study on the compressive behavior of micro-expansive ultra-high-performance concrete-filled steel tube columns, CONSTR BUILD MATER, 254 (2020) 119150, https://doi.org/10.1016/j.conbuildmat.2020.119150

[23] Hoang, A., Fehling, E.: Analysis of circular steel tube confined UHPC stub columns, STEEL COMPOS STRUCT, 23 (2017) 6, pp. 669-682, https://doi.org/10.12989/scs.2017.23.6.669

[24] Le Hoang, A., Fehling, E.: Numerical analysis of circular steel tube confined UHPC stub columns, COMPUT CONCRETE, 19 (2017) 3, pp. 263-273, https://doi.org/10.12989/cac.2017.19.3.263

[25] Chen, S., Zhang, R., Jia, L., et al.: Structural behavior of UHPC filled steel tube columns under axial loading, THIN WALL STRUCT, 130 (2018), pp. 550-563, https://doi.org/10.1016/j.tws.2018.06.016

[26] Xiong, M., Xiong, D., Liew, J.: Axial performance of short concrete filled steel tubes with high- and ultra-high-strength materials, ENG STRUCT, 136 (2017), pp. 494-510, https://doi.org/10.1016/j.engstruct.2017.01.037

[27] Lin, Z.: Researches on Behavior of RPC Filled Circular Steel Stub Axial Columns, M.Sc. Dissertation (2004), Fuzhou University, Fuzhou, China.

[28] Feng, J.: Study on mechanical behavior of reactive powder concrete filled steel tubular columns, M.Sc. Dissertation (2008), Tsinghua University, Beijing, China.

[29] Rong, Q., Zeng, Y., Hou, X., et al.: Finite element analysis and bearing capacity calculation for RPC-filled circular steel tube columns under axial compression, Journal of Harbin Institute of Technology, 22 (2018) 3, pp. 61-66, https://doi.org/10.11918/j.issn.0367-6234.201807186

[30] Wu, Y., Lin, Z.: Experimental study of behavior on RPC filled steel tubular stub columns under axial compression, China Jounal of Highway and Transport, 18 (2005) 1, pp. 57-62, https://doi.org/10.19721/j.cnki.1001-7372.2005.01.013